Assignment 1
Turbolence Modelling

Authors

Nicola Quaia - s232439
Gheorghi Battchiev - s233119

Contents

Introduction

The aim of this report is to conduct a detailed study of a fully developed one-dimensional turbulent flow in a channel and compare it with a laminar flow of the same type, which was analyzed during class lectures. A representation of the problem is shown in Figure 1. Due to the symmetry of the system, it is sufficient to focus the analysis on the lower half of the channel, from y=0 to y=H. This approach allows for a more efficient study while maintaining accuracy in understanding the flow behavior in the entire channel. Additionally, two turbulence models will be addressed: Prandtl's algebraic model and the $k-\epsilon$ model, to explore different approaches to describing the turbulent behavior of the flow.
To obtain the numerical solutions, several MATLAB functions have been developed.

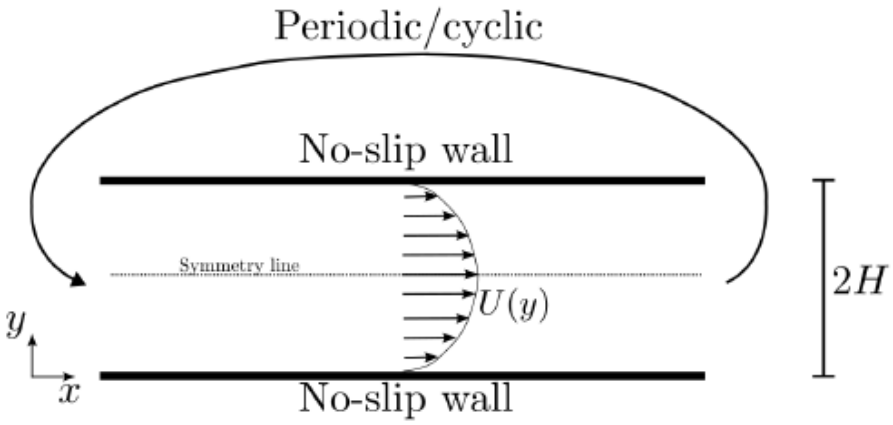

Figure 1: Schematic representation of the problem

1 Pressure Gradient in Fully Developed Turbulent 1D Flow

In order to derive an analytical relation for the pressure gradient, it is necessary to start from the Reynolds-Averaged Navier-Stokes (RANS) equations (Equation 1 and Equation 2) and reduce them to the relevant terms. Since the subject of the study is a fully developed one-dimensional flow in a channel, only the U-momentum equation is required.

$$\frac{\partial U_i}{\partial t} + U_j \frac{\partial U_i}{\partial x_j} = -\frac{1}{\rho}\frac{\partial P}{\partial x_i} + \nu \frac{\partial^2 U_i}{\partial x_j \partial x_j} - \frac{\partial u_i u_j}{\partial x_j} \tag{1}$$

$$U_{i,tot} = U_i + u_i \tag{2}$$

The velocity is decomposed in two components: U_i refers to the mean part while u_i represents the fluctuating part. It is possible to simplify Equation 1 as follows:

- A fully developed channel implies that: $\partial/\partial t = 0$.
- Velocities in the y and z-direction are equal to 0.
- The velocity U in the x-direction changes only in the y-direction, thus its derivatives in x and z are equal to 0: $\partial U/\partial x = 0$; $\partial U/\partial z = 0$.
- The pressure gradient is non zero only on the x-direction.

Additionally, for a channel flow, the following boundary conditions hold:

- at y = 0: U = 0 , know as the no-slip condition
- at y = H: $\frac{\partial U}{\partial y} = 0$, as the flow reaches its maximum in the middle of the channel

It follows that Equation 1 becomes:

$$\nu\frac{\partial^2 U}{\partial y^2} = \frac{1}{\rho}\frac{dP}{dx} + \frac{\partial \overline{uv}}{\partial y} \tag{3}$$

The only difference from the laminar case is the presence of the Reynolds stresses $\overline{uv}$. To derive an expression for the pressure gradient, $\overline{uv}$ can be expressed using the Boussinesq hypothesis, which relates the Reynolds stresses to the eddy viscosity and velocity (Equation 4). Moreover, the eddy viscosity is expressed using Prandtl's algebraic model.

$$\nu\frac{\partial^2 U}{\partial y^2} = \frac{1}{\rho}\frac{dP}{dx} + \frac{\partial}{\partial y}\left(-\nu_t\frac{\partial U}{\partial y}\right) \tag{4}$$

$$\nu\frac{\partial^2 U}{\partial y^2} = \frac{1}{\rho}\frac{dP}{dx} + \frac{\partial}{\partial y}\left(-{l_t}^2\left(\frac{\partial U}{\partial y}\right)^2\right) \tag{5}$$

$$\nu\frac{\partial^2 U}{\partial y^2} = \frac{1}{\rho}\frac{dP}{dx} + \frac{\partial}{\partial y}\left(-k^2y^2\left(\frac{\partial U}{\partial y}\right)^2\right) \tag{6}$$

Now, integrating Equation 6 with respect to y from y=0 to y=H results in Equation 1:

$$\nu\left(\left.\frac{\partial U}{\partial y}\right|_{y=H} - \left.\frac{\partial U}{\partial y}\right|_{y=0}\right) = \frac{1}{\rho}\frac{dP}{dx}H - \left(\left.k^2y^2|_{y=H}\left(\frac{\partial U}{\partial y}\right)^2\right|_{y=H}\right) + \left(\left.k^2y^2|_{y=0}\left(\frac{\partial U}{\partial y}\right)^2\right|_{y=0}\right) \tag{7}$$

The partial derivative of U with respect to y evaluated in y = H is equal to zero due to the boundary condition. It's also possible to cancel the far right term in the equation since y is evaluated at the wall.

$$-\nu \left.\frac{\partial U}{\partial y}\right|_{y=0} = \frac{1}{\rho}\frac{dP}{dx}H \tag{8}$$

From theory, it's also known:

$$\begin{cases} \tau_{wall} = \mu \left.\dfrac{\partial U}{\partial y}\right|_{y=0} \implies \left.\dfrac{\partial U}{\partial y}\right|_{y=0} = \dfrac{u_\tau^2}{\nu} \\ u_\tau = \sqrt{\dfrac{\tau_{wall}}{\rho}} \end{cases} \tag{9}$$

Finally the pressure gradient is found:

$$\frac{dP}{dx} = -\frac{\rho}{H}u_\tau^2 = -\frac{\rho\nu^2 Re_\tau^2}{H^3} \tag{10}$$

2 Development of a 1D Turbulent Channel Flow Solver

In this section, the objective is to develop a one-dimensional (1D) solver for the turbulent flow just described in the previous section. Two prominent turbulence closure models will be implemented: Prandtl's algebraic model and the k-epsilon model. These models will be employed to close the RANS equations, enabling effective predictions of turbulent flow characteristics. Specifically, the assignment will simulate flows at three distinct friction Reynolds numbers ($Re_\tau = 180, 395, 590$) to assess the impact of varying turbulence intensities on the flow profile. To validate the solver, results will be compared with Direct Numerical Simulation (DNS) data from [1] and [2].

2.1 Prandtl's Algebraic Model

Prandtl's algebraic model is a simplified turbulence modeling approach that predicts velocity profiles in turbulent boundary layers, particularly in wall-bounded flows. It is based on the logarithmic law of the wall, relating Reynolds stresses to velocity gradients through algebraic expressions. The model introduces a turbulent mixing length scale l_t and a turbulent velocity scale u_t to estimate turbulent kinetic energy k and turbulent viscosity ν_t. Prandtl's model is particularly effective in wall-bounded flows, such as channel or pipe flows, and is often used due to its computational efficiency and relatively simple implementation. However, it is less accurate in complex flows. Prandtl's model is described by the following relations:

$$\begin{cases} \nu_t = u_t l_t \\ u_t \approx l_t \left|\dfrac{\partial U}{\partial y}\right| \\ l_t = ky \quad \text{(wall bounded flow)} \end{cases} \tag{11}$$

As already seen in the previous section, by applying this model to the U-momentum equation it is possible to develop Equation 6. The pressure gradient can be substituted using

Equation 10, and the equation can be integrated with respect to y, resulting in Equation 12:

$$\nu\frac{\partial U}{\partial y} = -\frac{y}{H}u_\tau^2 - k^2y^2\left(\frac{\partial U}{\partial y}\right)^2 + C \tag{12}$$

By applying the boundary condition at y = H, it's possible to find that the integration constant C is equal to u_τ^2. It follows that:

$$\nu\frac{\partial U}{\partial y} = \left(1-\frac{y}{H}\right)u_\tau^2 - k^2y^2\left(\frac{\partial U}{\partial y}\right)^2 \tag{13}$$

At this point, it's necessary to nondimensionalize the equation and, in order to do that, the parameters proposed in Equation 14 are used:

$$\begin{cases} U^+ = \dfrac{U}{u_\tau} \\ y^+ = \dfrac{yu_\tau}{\nu} \\ Re_\tau = \dfrac{Hu_\tau}{\nu} \end{cases} \tag{14}$$

By appropriately substituting within Equation 13, Equation 15 can be obtained:

$$k^2{y^+}^2\left(\frac{\partial U^+}{\partial y^+}\right)^2 + \frac{\partial U^+}{\partial y^+} - \left(1-\frac{y^+}{Re_\tau}\right) = 0 \tag{15}$$

It is possible to solve the quadratic equation that has $\partial U^+/\partial y^+$ as the unknown:

$$\frac{\partial U^+}{\partial y^+} = \frac{-1+\sqrt{1+4k^2{y^+}^2\left(1-\frac{y^+}{Re_\tau}\right)}}{2k^2{y^+}^2} \tag{16}$$

Finally, finite differencing is applied with the forward scheme, resulting in Equation 17.

$$U^+(i+1) - U^+(i) = \left(\frac{-1+\sqrt{1+4k^2{y(i)^+}^2\left(1-\frac{y(i)^+}{Re_\tau}\right)}}{2k^2{y(i)^+}^2}\right)\Delta y \tag{17}$$

2.1.1 Van Driest Damping

When solving the U-momentum equation, in order to improve the solution, it's possible to introduce the Van Driest damping function to our turbulent mixing length l_t:

$$\begin{cases} l_t = ky\,f_\mu \\ f_\mu = (1-e^{-y^+/A^+}) \end{cases} \tag{18}$$

The damping function plays a crucial role in reducing eddy viscosity near the wall by modifying the turbulent viscosity to match the expected near-wall behavior in turbulent flows. In the viscous sublayer, where turbulence is minimal, the function effectively suppresses turbulence production by lowering turbulent viscosity. This adjustment allows the model to capture the sharp velocity gradient and accurately represent the reduced turbulence intensity near the wall. As a result, the damping function improves predictions of fully developed turbulent flow, particularly in one-dimensional (1D) and other configurations, by ensuring that near-wall effects are properly accounted for.

2.1.2 Comparison

Equation 17 can be implemented in the software with and without the damping function, for the various Re_τ, and compared to the reference data. The results are proposed in Figure 2, Figure 3 and Figure 4.
Near the wall (low y^+ values on the left side of the graphs), the lines overlap, indicating similar behavior across models. Further from the wall, the profiles diverge, with the damped function closely following the reference data. The effect of the Van Driest damping function on computing the mixing length (l_m) is displayed in Figure 5, and one can notice that the damping in more significant near the wall. However, since the implemented solution algorithm uses the "previous in space" result to compute the "next in space" value, a more correct estimation of the velocity profile next to the wall allows to "adjust the trajectory" of the solution, achieving a better estimation even far from the wall.

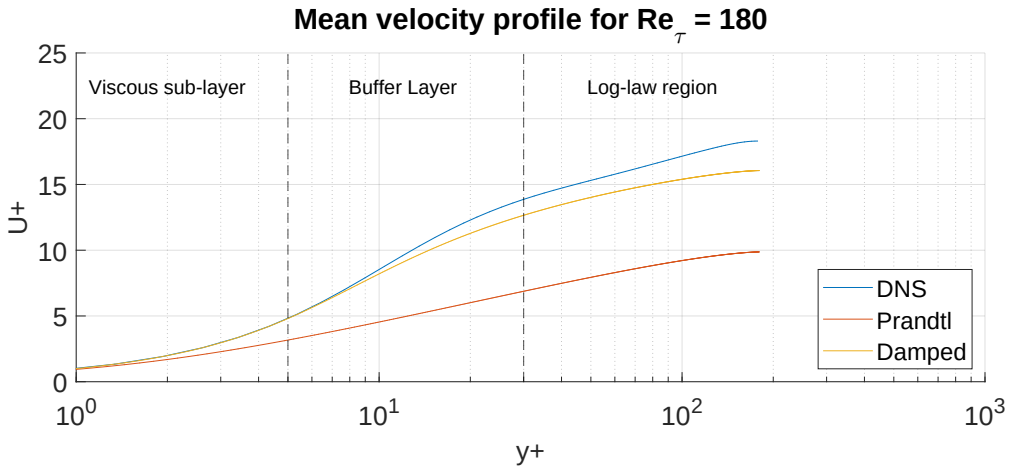

Figure 2: Comparison between DNS data from [2], Prandtl's model and Prandtl's model with damping function for $Re_\tau = 180$

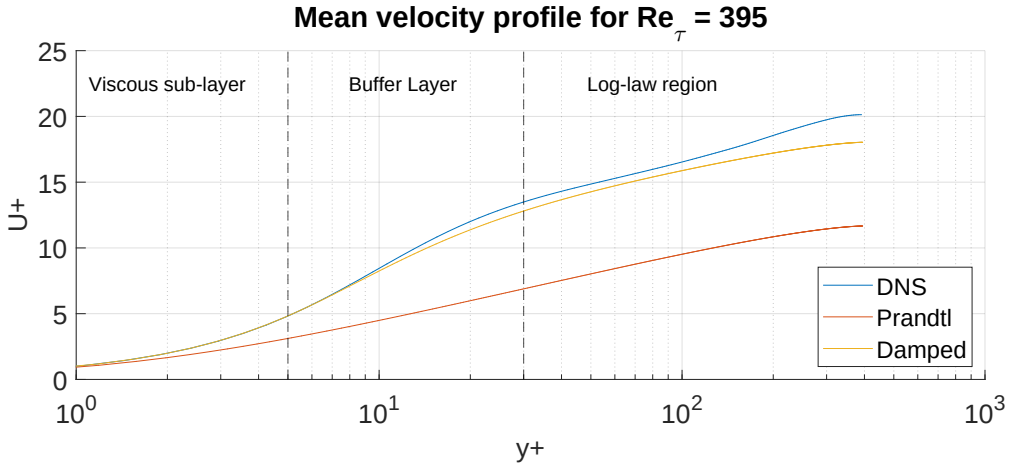

Figure 3: Comparison between DNS data from [2], Prandtl's model and Prandtl's model with damping function for $Re_\tau = 395$

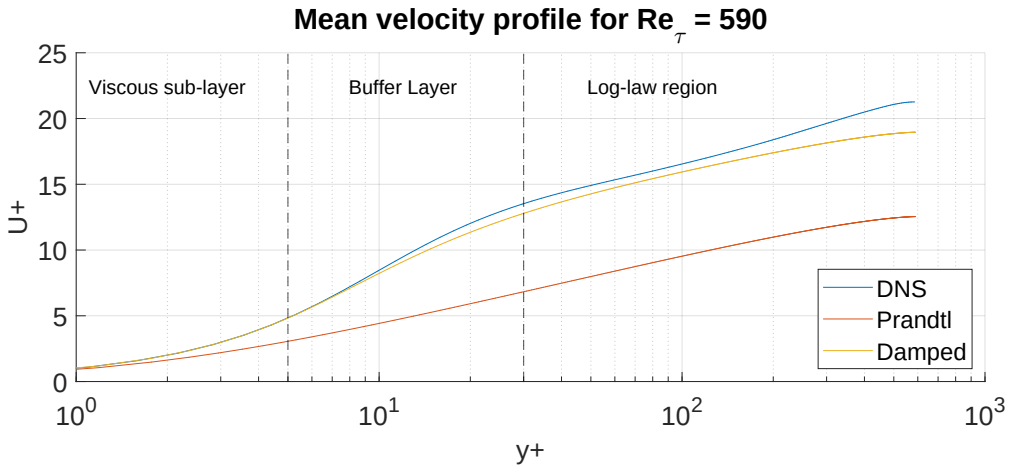

Figure 4: Comparison between DNS data from [2], Prandtl's model and Prandtl's model with damping function for $Re_\tau = 590$

2.1.3 Reynolds stresses

To develop an equation for the Reynolds stresses, one can again start from Equation 3, substitute the pressure gradient with the relation previously developed (Equation 10) and rearrange Equation 14 to normalize the equation. This results in Equation 19:

$$Re_{uv} = \frac{\overline{uv}}{u_\tau^2} = \frac{du^+}{dy^+} + \frac{y^+}{Re_\tau} - 1 \tag{19}$$

As $\partial u + /\partial y+$ was developed analytically in Equation 16, Re_{uv} can be simply computed without partial differencing or other numerical manipulations. The resulting graph is portrayed in Figure 6, showing the result without and with the damping function. Once again, the damping function allows to achieve a better similarity with the reference data.

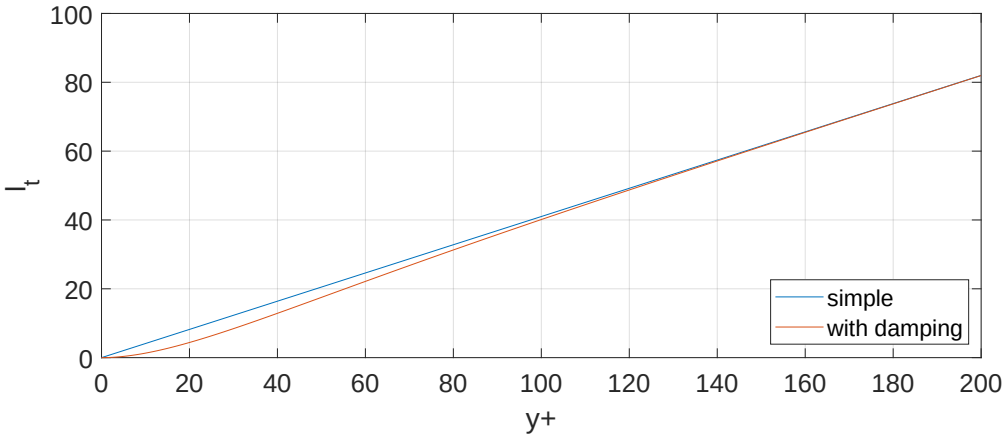

Figure 5: Comparison between mixing length of simple, wall-bounded flow and with the Van Dries damping function

Interestingly, this time the damping function has more effect on the first part of the graph. From Equation 19 and Equation 16, once can extrapolate that $Re_\tau \propto l_t$, so the damping function reduces the value of the curve at low $y+$.

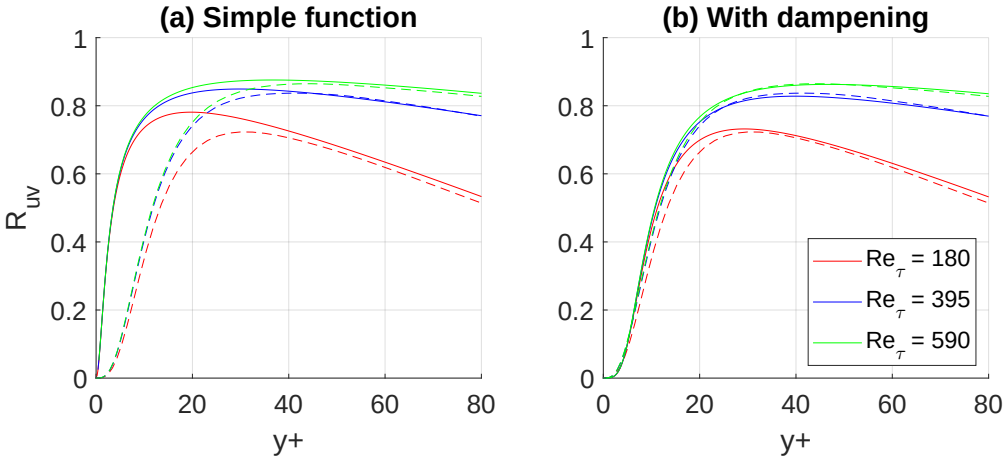

Figure 6: Reynold stresses for different Re_τ for the simple case (a) and with the damping function (b). Full line for the computed values, dashed for the reference data

2.1.4 Additional analysis

To evaluate the accuracy of the numerical solution, it is important to analyze the effect of varying the number of grid points. In Figure 7, the basic Prandtl model is evaluated using grid sizes of n = 10, 100, 1000, and 10000. It is clear that the computed velocity profile is sensitive to the number of grid points: values of n $<$ 1000 are too coarse to yield reliable results. Since the difference between n = 10^3 and n = 10^4 is negligible, an optimal value of n = 1000 is chosen. This grid size has been used in the previous graphs and will continue to be used in those that follow.

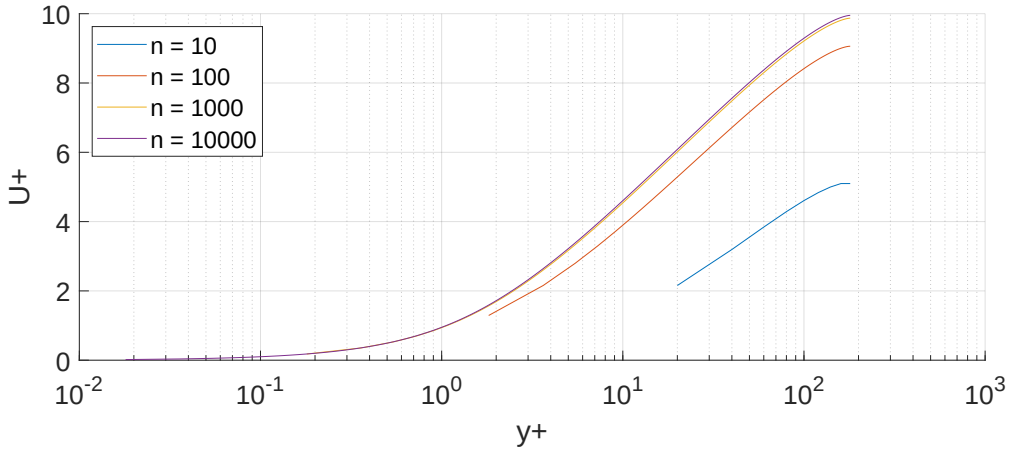

Figure 7: Simple Prandtl function for different numbers of grid points.

For completeness, a comparison between the various Re_τ was also conducted and reported in Figure 8. One can see that the resulting velocity profiles are similar close to the wall but, for large y+, higher friction Reynolds numbers yield larger values.

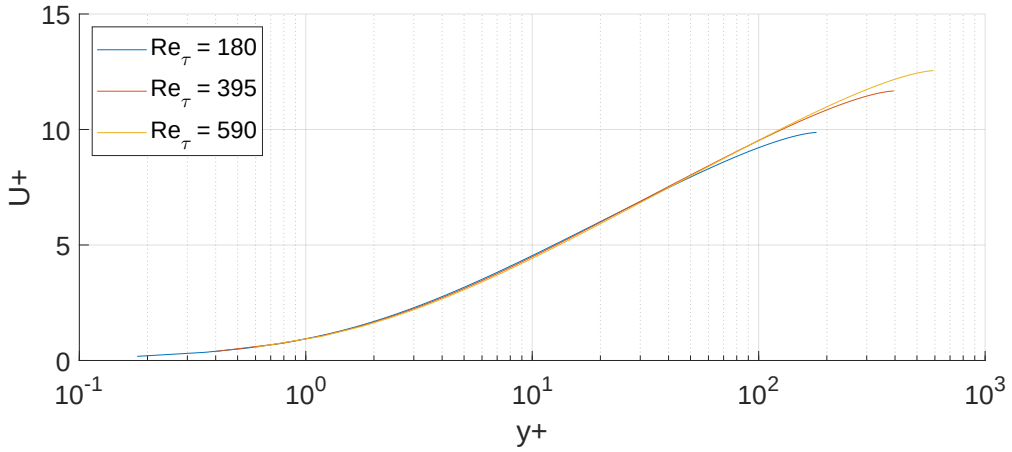

Figure 8: Simple Prandtl function for different numbers of grid points.

2.2 K-Epsilon Model

The k-ϵ model is a two equations model, as it is developed by solving the transport equation for the turbulent kinetic energy (TKE), k (Equation 20) and the rate of dissipation of turbulent kinetic energy, ϵ (Equation 21) simultaneously [3].

$$\frac{\partial(\rho k)}{\partial t} + \frac{\partial(\rho U_i k)}{\partial x_i} = \frac{\partial}{\partial x_j}\left[\left(\mu + \frac{\mu_t}{\sigma_k}\right)\frac{\partial k}{\partial x_j}\right] + P_k - \rho\epsilon + S_k \tag{20}$$

$$\frac{\partial(\rho \epsilon)}{\partial t} + \frac{\partial(\rho U_i \epsilon)}{\partial x_i} = \frac{\partial}{\partial x_j}\left[\left(\mu + \frac{\mu_t}{\sigma_\epsilon}\right)\frac{\partial \epsilon}{\partial x_j}\right] + C_1\frac{\epsilon}{k}P_k - C_2\rho\frac{\epsilon^2}{k} + S_\epsilon \tag{21}$$

As described before, for a 1D fully developed channel flow, some assumptions can be made to simplify these equations. In addition, the terms S_k and S_ϵ, which represent a TKE sink and a dissipation of TKE sink, can be considered zero. Hence the transport equations can be rewritten as Equation 22 and Equation 23.

$$\frac{\partial}{\partial y}\left(\nu + \frac{\nu_T}{\sigma_k}\frac{\partial k}{\partial y}\right) = \epsilon - \frac{P_k}{\rho} \tag{22}$$

$$\frac{\partial}{\partial y}\left(\nu + \frac{\nu_T}{\sigma_\epsilon}\frac{\partial \epsilon}{\partial y}\right) = C_2\frac{\epsilon^2}{k} - C_1\frac{\epsilon}{k}\frac{P_k}{\rho} \tag{23}$$

Additionally, Equation 24 can be derived from Equation 4.

$$\frac{\partial}{\partial y}\left(\nu + \nu_T\frac{\partial U}{\partial y}\right) = \frac{1}{\rho}\frac{\partial P}{\partial x} \tag{24}$$

Moreover, the eddy viscosity ν_T is defined by Equation 25. Finally, using the Boussinesq hypothesis, the TKE production rate can be derived following Equation 26.

$$\nu_T = f_\mu C_\mu \frac{k^2}{\epsilon} \tag{25}$$

$$P_k = -\rho\overline{uv}\frac{\partial U}{\partial y} \quad \rightarrow \quad P' = \frac{P}{\rho} = \nu_T\left(\frac{\partial U}{\partial y}\right)^2 \tag{26}$$

For simplicity, P' is written simply as P from this point onwards.
Hence, finite differencing can be applied to the Equations from 22 to 26, resulting in the system of equations proposed in Equation 2.2.

$$\begin{cases} \nu_{T_i} = C_\mu \dfrac{k_i^2}{\epsilon_i} \\ P_i = \nu_{T_i}\left(\dfrac{U_{i+1} - U_{i-1}}{2\Delta y}\right)^2 \\ \left[(2\nu + \nu_{T_{i+1}} + \nu_{T_i})U_{i+1} + (-4\nu - \nu_{T_{i+1}} - 2\nu_{T_i} - \nu_{T_{i-1}})U_i + (2\nu + \nu_{T_i} + \nu_{T_{i-1}})U_{i-1}\right] \\ \qquad = 2\Delta y^2 \dfrac{1}{\rho}\dfrac{dP_0}{dx} \\ \left[(2\nu + \nu_{T_{i+1}} + \nu_{T_i})k_{i+1} + (-4\nu - \nu_{T_{i+1}} - 2\nu_{T_i} - \nu_{T_{i-1}})k_i + (2\nu + \nu_{T_i} + \nu_{T_{i-1}})k_{i-1}\right] \\ \qquad = 2\Delta y^2 \sigma_k[\epsilon_i - P_i] \\ \left[(2\nu + \nu_{T_{i+1}} + \nu_{T_i})\epsilon_{i+1} + (-4\nu - \nu_{T_{i+1}} - 2\nu_{T_i} - \nu_{T_{i-1}})\epsilon_i + (2\nu + \nu_{T_i} + \nu_{T_{i-1}})\epsilon_{i-1}\right] \\ \qquad = 2\Delta y^2 \sigma_\epsilon\left[C_2\dfrac{\epsilon_i^2}{k_i} - C_1\dfrac{\epsilon_i}{k_i}P_i\right] \end{cases} \tag{27}$$

Then, the system can be solved iteratively. From a first, arbitrary guess, the 5 quantities (ν_T, U, P, k, ϵ) can be inserted in the formulae to evaluate the new quantities. This process

can be repeated until the RMS error between the U_{new} and U is less than a defined tolerance, or the loop has been run more than a maximum number of iterations. The constant values previously mentioned are defined in Table 1. Additionally, the parameter f_μ can be set to Equation 2.1.1 to apply the dumping function.

quantity	C_μ	C_1	C_2	σ_k	σ_ϵ	f_μ	A^+
value	0.09	1.45	1.9	1	1.3	1	26

Table 1: Parameter values for k-epsilon model

The MATLAB output is displayed in Figure 9, and a zoom of the top-rightmost part is presented in Figure 10. Unfortunately, the implementation does not provide a satisfactory result: the general shape follows the same trend as the other graphs previously described, but the magnitude is off. Regarding the comparison between the model with and without the damping function, it is possible to notice an improvement for larger $y+$, as expected.

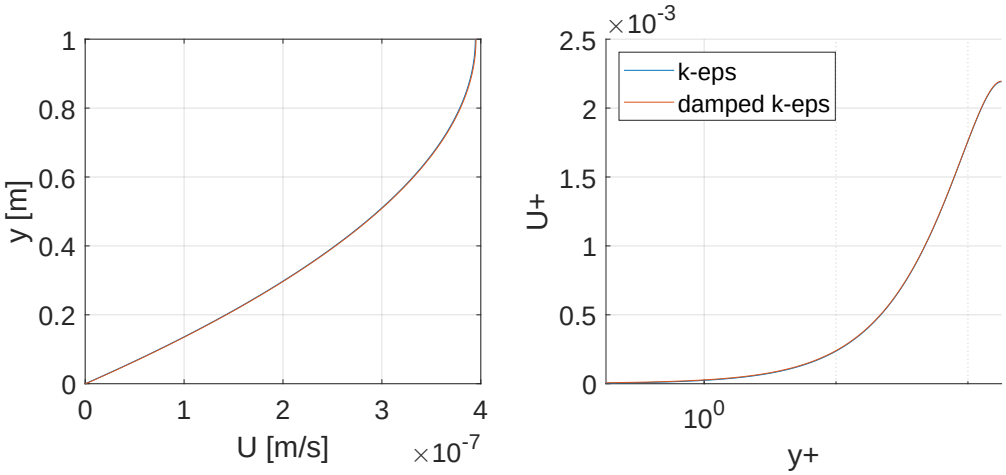

Figure 9: Flow evaluated using the k-ϵ model

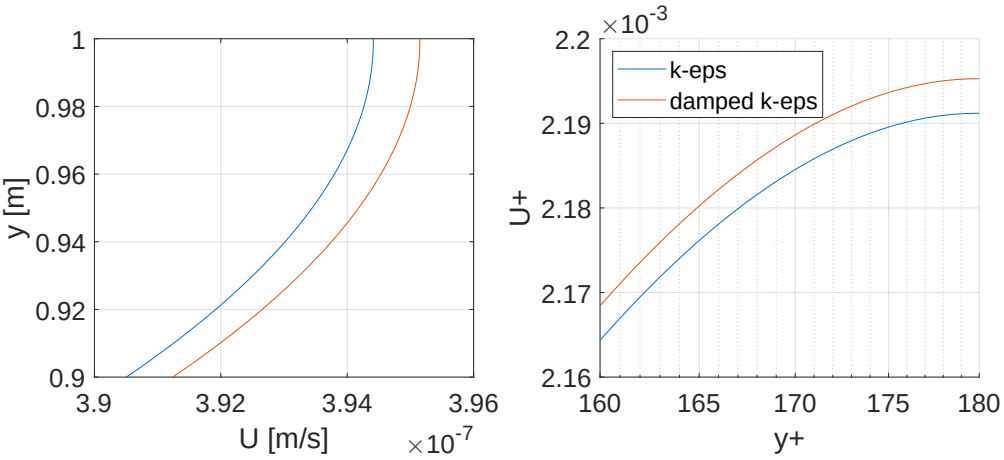

Figure 10: Zoom of the flow evaluated using the k-ϵ model

3 Comparison between turbulent and laminar

To compute and compare the velocity profiles between the turbulent and laminar cases, it is essential to maintain consistent physical parameters and apply the same boundary conditions. To enable a fair comparison, Equation 3 was solved, substituting the pressure gradient found in Equation 10, for both the turbulent and laminar cases.
For the laminar case, it is straightforward to integrate twice with respect to y to obtain the following analytical expression:

$$U_{lam} = \frac{u_\tau^2}{\nu}\left(y - \frac{y^2}{2H}\right) \tag{28}$$

For the turbulent case, an analogous procedure to the one implemented in subsection 2.1 was implemented to find $\partial U/\partial y$; subsequently, the velocity was calculated using finite differencing with a forward scheme (Equation 29). The results are shown in the Figure 11. Note that the turbulent profile is multiplied by a factor of 5 to allow easier readability.

$$U(i+1) - U(i) = \left(\frac{-\nu + \sqrt{\nu^2 + 4k^2 y(i)^2 u_\tau^2 \left(1 - \frac{y(i)}{H}\right)}}{2k^2 y(i)^2}\right)\Delta y \tag{29}$$

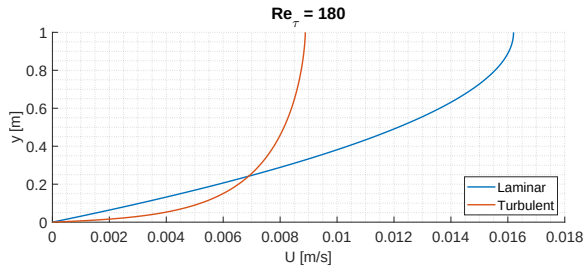

(a) (a)

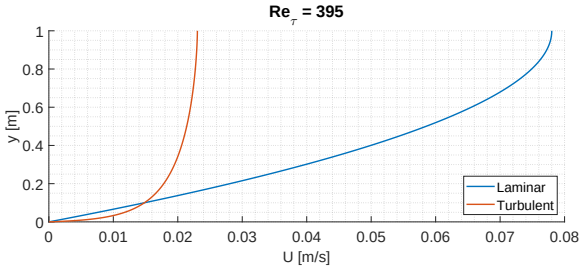

(b) (b))

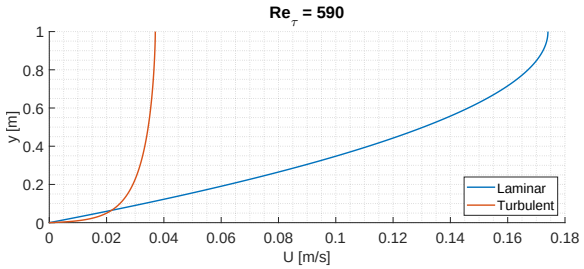

(c) (c)

Figure 11: Velocity profiles comparison for different values of Re_τ:
a) $Re_\tau = 180$; b)$Re_\tau = 395$; c)$Re_\tau = 590$

The results align with the expected behavior of laminar and turbulent flows. Near the wall, the turbulent flow exhibits a steeper velocity gradient, indicating a rapid increase in velocity compared to the laminar flow. This behavior is characteristic of turbulent flows, which experience higher shear stress and momentum exchange close to the boundary. Conversely, farther from the wall and especially toward the center of the channel, the laminar flow reaches a higher velocity than the turbulent flow. This is expected because laminar flow distributes velocity more uniformly across the channel.

4 Conclusion

Throughout the report, the turbulent and laminar flow is analyzed for a 1D, fully developed channel flow. Firstly, the pressure gradient is derived as a function of u_τ, H and ρ. Secondly the flow is numerically solved using the Prandtl's algebraic model and the k-ϵ model for various Re_τ and compared to the reference data. The profiles are plotted in a semi-log format as many relations can be expressed throughout the so-called log law (Equation 4), which becomes cleared in a semi-log format, as can be seen in Figure 12.

$$u^+ = \frac{1}{k} ln(y^+) + B \tag{30}$$

The effect of the damping function is also analyzed. To sum up, this function provides a better estimation in the near-wall region, and this "better start" allows to achieve an overall

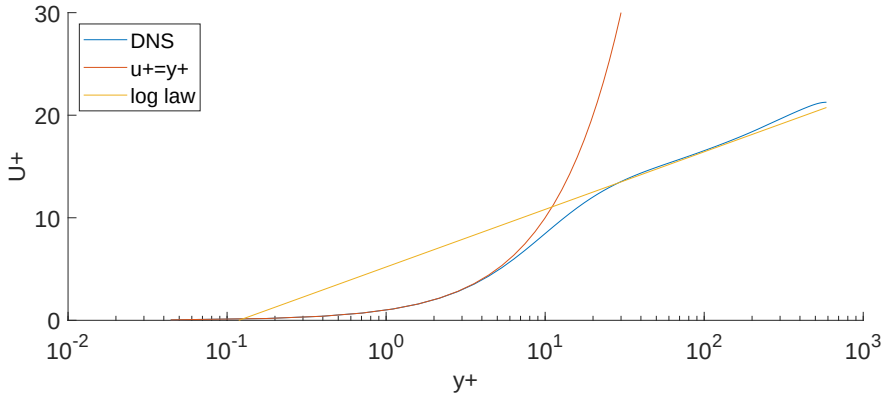

Figure 12: Wall flow relations at $Re_tau = 590$. Log law taken from [1].

better result if a finite differencing approach is used.
Unfortunately, the application of the k- ϵ model did not produced satisfactory results, and it is not possible to compare it with the reference data or the other model.
On the contrary, the comparison with the laminar flow was successful: the turbulent profile increases more rapidly, but in the center of the channel the laminar flow is faster.

In conclusion, Prandtl's algebraic model proved relatively straightforward to implement and quick to solve, although the results diverged significantly from the reference data. Incorporating the damping function, which adds minimal computational complexity, led to significant improvements in flow predictions. While the k-ϵ model theoretically promises better results, its complexity may be excessive for this relatively simple flow analysis.

5 Acknowledgements

To develop the report, ChatGPT was used to help in developing the code, especially for plotting and debugging, and was marginally used to rewrite the text, check the spelling, and improve the English.

6 Contributions

The work was divided equally among the members. In particular, the work was divided as follows:

- Nicola Quaia - s232439: main coder, developing k-eps model, final checking.
- Gheorghi Battchiev - s233119: main derivation, main reporter, laminar vs turbulent analysis.

References

[1] John Kim, Parviz Moin, and Robert Moser. Turbulence statistics in fully developed channel flow at low reynolds number. *Journal of Fluid Mechanics*, 177:133â166, 1987.

[2] Robert D. Moser, John Kim, and Nagi N. Mansour. Direct numerical simulation of turbulent channel flow up to ReĎ=590. *Physics of Fluids*, 11(4):943–945, 04 1999.

[3] H. K. Versteeg and W. Malalasekera. *An Introduction to Computational Fluid Dynamics: The Finite Volume Method*. Pearson Education Ltd., Harlow, England, 2nd edition, 2007.